Solid-State NMR Investigation of Cold-Flow Properties of Hydrotreated Vegetable Oils and Their Blends with Petroleum Diesels

Ségolène Laage, Maria Rappo, Audrey Pleynet, Aleksandra Lelevic, Aurélie Borel, Simon Pondaven, Cédric Lorthioir

HAL Id: hal-04733864
https://hal.sorbonne-universite.fr/hal-04733864v1

Solid-state NMR investigation of cold-flow properties of hydrotreated vegetable oils and their blends with petroleum diesels

Ségolène Laage[1]*, Maria Rappo[1], Audrey Pleynet[1], Aleksandra Lelevic[1], Aurélie Borel[1], Simon Pondaven[1], Cédric Lorthioir[2]

(1) TotalEnergies, Centre de Recherche de Solaize (CRES), Chemin du canal, BP 22,

69360 Solaize, France

(2) Sorbonne Université, CNRS, Laboratoire de Chimie de la Matière Condensée de Paris,

LCMCP, UMR 7574, 75005 Paris, France

*Email : segolene.laage@totalenergies.com

ABSTRACT.

The cold flow properties of hydrotreated vegetable oils (HVO) and of their blends with petroleum diesel were investigated by solid-state NMR (SSNMR). The fraction of protons in the crystallites was successfully determined at temperatures going from 30°C to -50°C, offering a

way to precisely monitor the crystallization process occurring during the cool-down of hydrocarbons. The Magic-Sandwich Echo experiment used in this work displayed a higher sensitivity compared to other methods such as cloud point, pour point and cold filter plugging points, with a detection of the onset of crystallization by SSNMR up to 15°C with respect to other techniques. The properties of three distinct HVO and of their blends with a petroleum diesel were determined and related to their detailed chemical composition. Results showed that a high branching level was the primary factor impacting the onset of crystallization of the HVO. The carbon number distribution was observed to impact the rate of crystallization as a function of temperature. Lastly, blending petroleum diesel with HVO was demonstrated to keep the cold-flow properties of the diesel unchanged at 10 wt % mixing. In contrast, a shift of the cold-flow properties of the blends towards the HVO behavior was detected at 30 wt % and 50 wt % mixing, with either a negative or positive impact depending on the chemical composition of the added HVO.

1. INTRODUCTION

Biofuels are considered as an attractive option to limit the greenhouse gas emissions in the transport sector, which was responsible for 27% of these emissions in Europe in 2017 [1]. Among biofuels, hydrotreated vegetable oils (HVO) display significant advantageous properties for the engine and the environment which make them better candidates than diesels for several applications. HVO have high cetane number, low density, lower heating value and better oxidative stability than diesels. Their properties can be adjusted by modifying the parameters of their preparation reaction, such as temperature, pressure, and the nature of the catalyst used so that they meet various industrial needs. The major drawbacks of HVO stand in their poor low-temperature properties, which could hamper their use at high blending percentage for combustion-ignition engines. Indeed, poor engine performance and high NO_x emissions are likely to occur when diesel with poor cold-flow properties are used in direct injection diesel engines [2,3]. The upgrading technology of cold-flow properties of HVO reported in the literature include isomerization and blending with petroleum diesel [4].

Nuclear Magnetic Resonance (NMR) is here suggested as a versatile technique to investigate the temperature-dependent behavior of three different HVO and to correlate their cold properties with their chemical composition. The methodology presented here characterizes both the behavior of pure HVO, but also investigates their impact on the low-temperature behavior of petroleum diesels at blending percentages ranging from 10 wt % to 50 wt %.

Other analytical techniques have been proposed in the literature to monitor the crystallization phenomenon occurring at low temperature [4,5]. Differential scanning calorimetry (DSC) can detect the exothermic onset of wax crystallization upon cooling and can indirectly deduce the percentage of wax from the released amount of heat. The sensitivity of DSC is however directly

related to the cooling/heating rate and reduction of this rate can compromise identification of the onset of crystallization [6,7]. Near infrared spectroscopy combined with chemometric tools has also been used to predict cold-flow properties of diesels and blends [8–11]. However, this last method is strongly dependent on the database used for the chemometric analysis. The solid-state NMR (SSNMR) technique presented here is highly robust and can be applied to any proton-bearing species. It is also significantly more sensitive than the classical physical tests used to quantify the cold-flow properties of fluids, as illustrated by the early onset of crystallization detected by SSNMR compared to other techniques. Lastly, the ability to cool down the probe at an accurate temperature value makes SSNMR a well-suited tool to monitor the rate and slope of crystallization as a function of temperature. The experiments presented here were carried out on a high magnetic field spectrometer. However, since resolution is not critical for the presented relaxation measurements, their transposition to benchtop spectrometers with lower field is completely possible [12–15]. Such experiments can therefore easily be implemented on standard laboratory equipment.

2. EXPERIMENTAL SECTION

2.1. Materials

The petroleum diesel used to prepare blends with different HVO fulfills the EN 590 specifications. The key characteristics of this petroleum diesel are detailed in Table 1.

Table 1. Characteristics of the reference diesel

	CP (°C)	CFPP (°C)	PP (°C)	Density at 15°C (kg/m³)	Kinetic viscosity at 40°C (mm²/s)	Atmospheric Distillation test					
	ASTM D7689	EN 116	ASTM D7346	EN ISO 12185	EN ISO 3104	ASTM D86					
Reference diesel	- 3	-2	-12	831.2	3.21	Initial Boiling Point (°C)	Final Boiling Point (°C)	Temperature 95% (V/V) recovered (°C)	Distilled volume (mL)	Residue (mL)	Losses (mL)
						166.8	359.1	253.6	97.9	1.5	0.6

Three HVO were considered in this work. Although paraffins are the main components of HVO, chains with unsaturations and branches are also present. Variations in the chain length, level of unsaturated chains and isomerization profiles can be observed between the three selected HVO as described below.

The HVO preparation process consists of a hydrotreatment of vegetable oil and then an isomerization of the C16~C18 paraffinic material. During the hydrotreatment, the triglycerides of the vegetable oil are converted into hydrocarbons through a hydrogenation reaction. Hydrogen is used to remove the oxygen from the triglycerides producing a mix of linear paraffins, carbon dioxide and water. Then, the product of hydrotreatment is isomerized, always in presence of hydrogen, in order to create branching along the linear chains and to improve, by this way, the cold-flow properties of the final products. Thus, HVO are obtained free of sulphur and aromatics and with a very high cetane number.

The ratio of n-paraffins and iso-paraffins varies to an extent which depends on the conditions of the isomerization process. This ratio was determined by two-dimensional Gas-Chromatography with FID detector for each investigated HVO (see Supporting Information).

The following diesel fuel samples refer to either pure petroleum diesel, HVO samples, or blends of HVO with the investigated petroleum diesel.

2.3. ^{1}H Solid-State NMR

The SSNMR experiments were carried out on a Bruker Avance III HD NMR spectrometer coupled to a NMR magnetic field of 7.05 T and equipped with a 4 mm double-resonance ^{1}H-X MAS probe head. The samples were introduced into a Kel-F insert for 4 mm MAS rotors, closed by a sealing screw. The measurements were performed without any magic-angle spinning (MAS) of the samples. The ^{1}H transverse relaxation signal was recorded using the Magic Sandwich Echo (MSE) pulse sequence represented in Figure 1, with a 90°(^{1}H) pulse length equal to 2.3 μs and a number of sandwich blocks, n_{MSE}, ranging from 1 to 20. The recycle delay was adjusted taking into account the evolution of the ^{1}H spin-lattice relaxation time, T_1(^{1}H), in the probed temperature range (223 K – 303 K): the highest value of this delay amounted to 12 s.
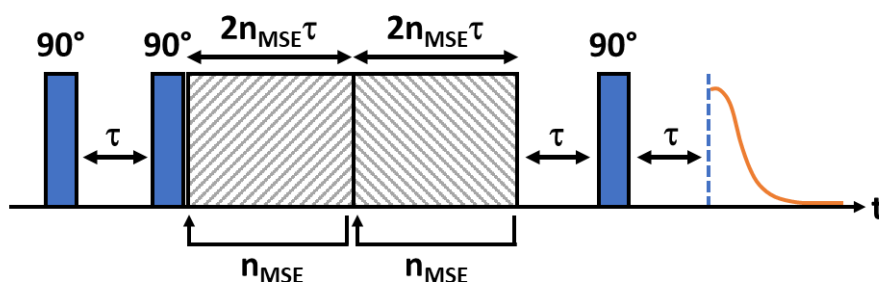
Figure 1. Schematic representation of the Magic-Sandwich Echo (MSE) pulse sequence. The first sandwich block corresponds to [t_0-90°-$2t_0$-90°-$2t_0$-90°-$2t_0$-90°-t_0] and the second one, to the mirrored sequence with inverted phases compared to the pulses of the first block. The delay t_0 stands for the phase switching time. The phase cycling is described in detail in [16]. n_{MSE} denotes the number of MSE cycles applied before the detection of the ^{1}H NMR signal.

For each sample and at each temperature, the sample was first heated at 60°C in order to remove its thermal history. Then, the rotor was inserted in the NMR probe head, which was

previously equilibrated for 10 min at the temperature of interest, and the NMR data were recorded just after the sample insertion. For some of the samples, the rotor was let in the NMR magnet after the initial measurement and the same experiment was repeated after 10 min, 20 min and 30 min, under the same experimental conditions. Such a protocol allowed to check that the crystalline fraction formed in the diesel fuels does not vary over this time scale.

2.4. Fitting procedure for the ^{1}H transverse relaxation functions

The MSE pulse sequence allows the fraction of protons involved in molecular moieties that are immobile over the tens of microseconds time scale to be quantified in an accurate manner. Such protons indeed give rise to a fast-relaxing component that may be observed during the first 200 microseconds of the ^{1}H transverse relaxation function. The MSE experiment provides the opportunity to detect the occurrence of such a component and to determine the proportion of these protons with respect to the total number of protons in the investigated samples.

The protons from the crystallites formed during the cooling of diesels are characterized by strong ^{1}H-^{1}H dipolar couplings D_{HH} that are not, or almost not, averaged by molecular motions. As a result, the ^{1}H transverse relaxation function M(t) displays a fast relaxation component which may be observed over the first 20 microseconds, with a Gaussian or Abragam-like shape. At longer time, only the protons from the mobile phase of the partially crystallized diesel contribute to M(t). Assuming a two-phase description of the cooled system, M(t) may be expressed using the following equation:

$$M(t) = M_0 \times \left[f_R \times e^{-at^2/2} + (1 - f_R) \times e^{-(t/T_2)^\beta} \right] \qquad (1)$$

In this expression, M_0 stands for the ^{1}H magnetization of the sample at equilibrium, f_R corresponds to the fraction of protons in the crystallites while under the second-moment approximation, the parameter a is proportional to D_{HH}^2. The last term of eq 1 is used to describe the contribution from the protons located in the mobile phase. It should be remarked that a stretched exponential was considered because it allows a satisfactory description of the ^{1}H transverse relaxation, as will be shown in the following. Such a function allows to reflect the fact that the fuels considered are intrinsically complex fluids that are not characterized by a single ^{1}H T_2 relaxation time. Nevertheless, the stretched exponential also accounts for the curvature of $M(t)$ in the time regime between 20 µs and 200 µs that partly results from the different ^{1}H chemical shift values of the chemically distinct protons from the diesel.

In some cases, a weak fraction of the diesel protons is involved in crystalline regions. For this reason, the MSE experiment was preferred to the solid-echo pulse sequence. Indeed, at each temperature, the ^{1}H transverse relaxation signal was recorded following different number of MSE cycles, n_{MSE}, ranging between 1 and 20. Above $n_{MSE} = 9$-10 typically, only the mobile protons contribute to the corresponding MSE signal. These latter were successfully described using a stretched exponential, imposing a common value for T_2 and β. In a second step, the parameters T_2 and β thus obtained were then fixed for the fit of the MSE data obtained for $n_{MSE} = 1$. Such an approach, proposed by [13], allows to make the fitting procedure more robust and to get more accurate values of f_R, even in the case of samples with few crystallites. An example of the ^{1}H MSE signal obtained in the case of a petroleum diesel and its fit is represented on Figure 2 for illustration.
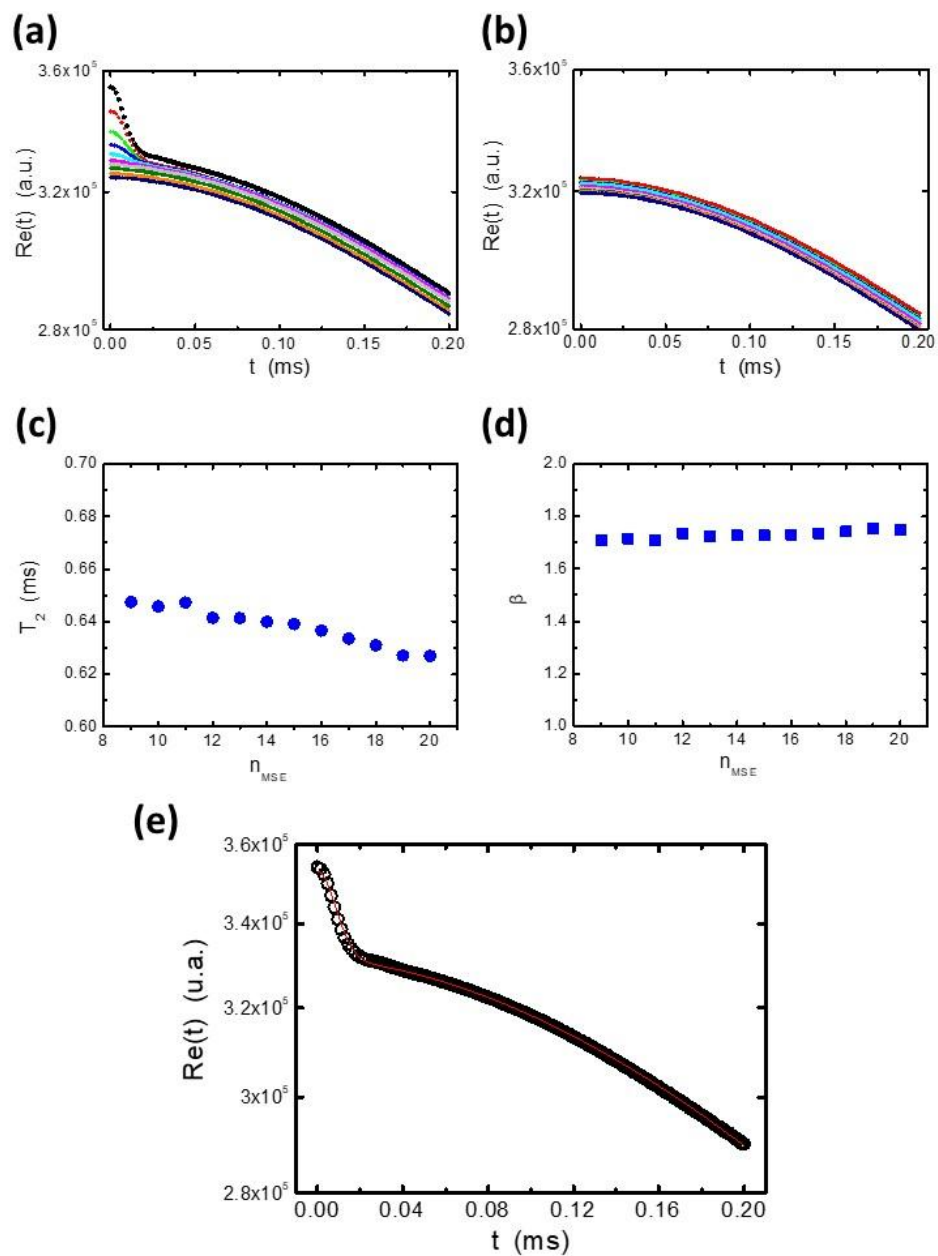
Figure 2. [1]H MSE signals determined on a representative petroleum diesel according to EN 590 at -25°C, for various MSE cycles, n_{MSE}: n_{MSE} is increased (a) from 1 to 10 and (b) from 11 to 20. Evolution of (c) the relaxation time T_2, and (d) the stretching exponent, β, describing the MSE signals recorded for n_{MSE} above 10. (e) Fit of the MSE signal obtained for $n_{MSE} = 1$, by constraining both T_2 and β values to the ones obtained above $n_{MSE} = 10$.

3. RESULTS

Figure 3 shows the temperature dependence of the rigid fraction, f_R, obtained for a petroleum diesel which will serve, in the following, as a common basis to prepare the blends with each of the three considered HVO. At this stage, one may note that the evolution $f_R(T)$ was found to be the same, independently of the cooling mode, as shown in Figure S8. For this neat diesel, f_R is equal to 0 from room temperature down to ~5°C. An almost linear increase of f_R is then observed from 5°C to -40°C with a final f_R value of about 10%, as shown in Figure 3. Therefore, the temperature dependence of f_R displays an onset of crystallization followed by a progressive crystallization process as the diesel is cooled down. Such behavior is consistent with the crystallization rate expected for a regular diesel with a broad distribution of carbon number. This distribution ranges between 7 and 30 carbons per chain as displayed in the Supporting Information. Optical microscope analyses were performed on the same reference and the formation of the first visible crystals was observed around 4°C (Figure S5). Such feature is consistent with the NMR data, which allow the detection of crystallites even though their characteristic size stands below a few hundred nanometers. These results show that the MSE experiment is an accurate approach to investigate the crystallization-behavior upon cooling.
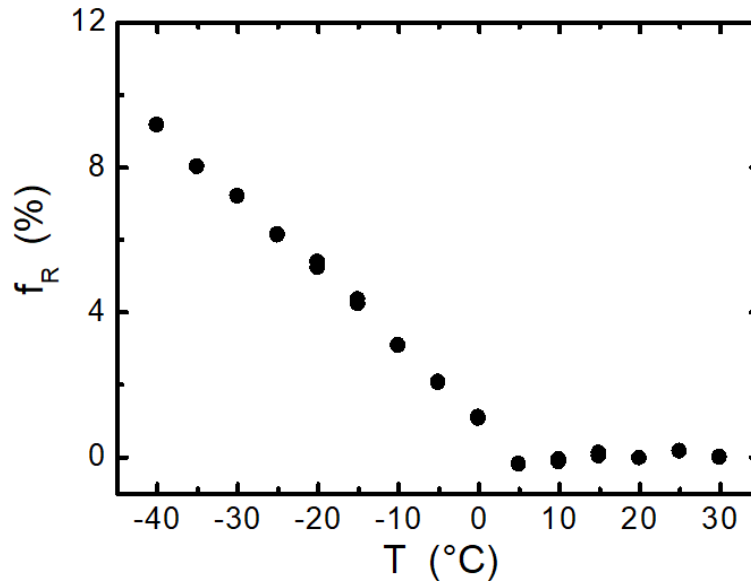
Figure 3. Temperature dependance of the fraction of protons involved in the crystallites formed under isothermal crystallization. Before each measurement, the sample temperature was increased at 60°C.

The same NMR methodology was applied for the three pure HVO samples from different origins and molecular compositions. No significant rigid fractions were observed between 30°C and 0°C for HVO 1 and 2, before displaying a sharp and linear increase of the rigid fraction between 0°C and -30°C. Towards low temperatures, a plateau was observed between -30°C and -50°C with final rigid fractions around 20 % and 16 % for HVO 1 and 2, respectively.

HVO 3 displayed a very different pattern as compared to the first two ones with no significant rigid fractions between room temperature and -30°C. Below -30°C to -50°C, a linear increase of the f_R is observed with a final value around 6%. No plateau was reached for HVO 3 at -50°C. These results evidenced very different cold properties between HVO 1 and 2 on the one hand and HVO 3 on the other hand. The sharper increase of the rigid fraction for HVO 1 and 2 displayed in Figure 4 (from 0°C to -30°C) compared to the one observed for the petroleum diesel in Figure

3 (from 0°C to -40°C) is to be related to their well-centered and narrow distribution of paraffins around the C16-C18 populations while the petroleum diesel displays a broader carbon distribution from C7 to C30.

As for the diesel reference, additional tests were performed using optical microscopy on the three HVO samples and over the same temperature range. The results (Figure S6) showed that with decreasing temperatures, the first crystals appeared at, respectively, -7°C and -10°C for HVO 1 and 2. On the other end, the first observable crystals for HVO 3 were observed around -38°C, confirming the same trends and differences derived from the NMR data.
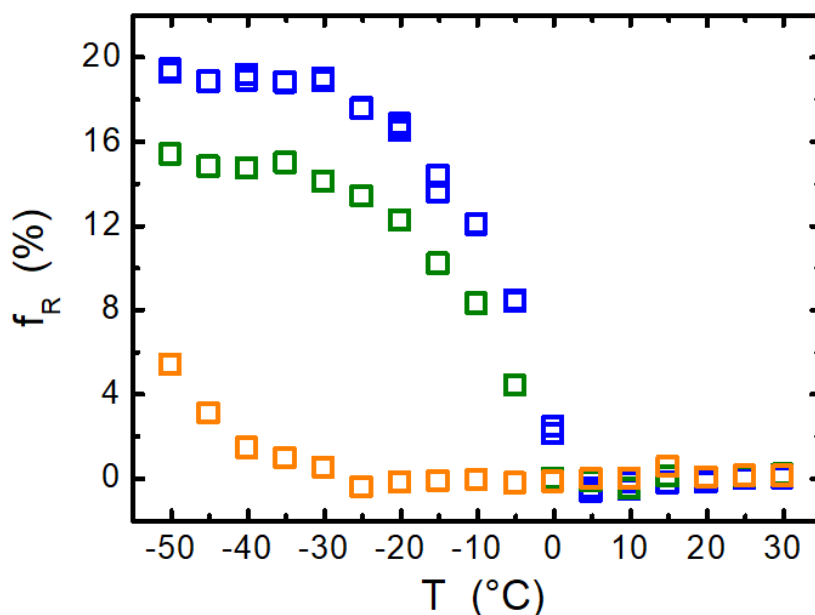
Figure 4. Evolution of the fraction of protons contributing to the crystallites resulting from the isothermal crystallization of HVO 1 (□), HVO 2 (□) and HVO 3 (□). All the samples were heated at 60°C before any measurement.

Finally, ^{1}H NMR relaxation approaches were applied to mixed samples based on the petroleum diesel reference. 10%, 30% and 50% of each HVO were diluted in the reference diesel and analyzed following the same NMR protocol as described above. The experimental rigid fractions

and their temperatures dependance are shown in Figure 5 for diesel/HVO blends prepared for each HVO, introduced in various contents. In each graph, the data related to the reference diesel were also added for comparison.
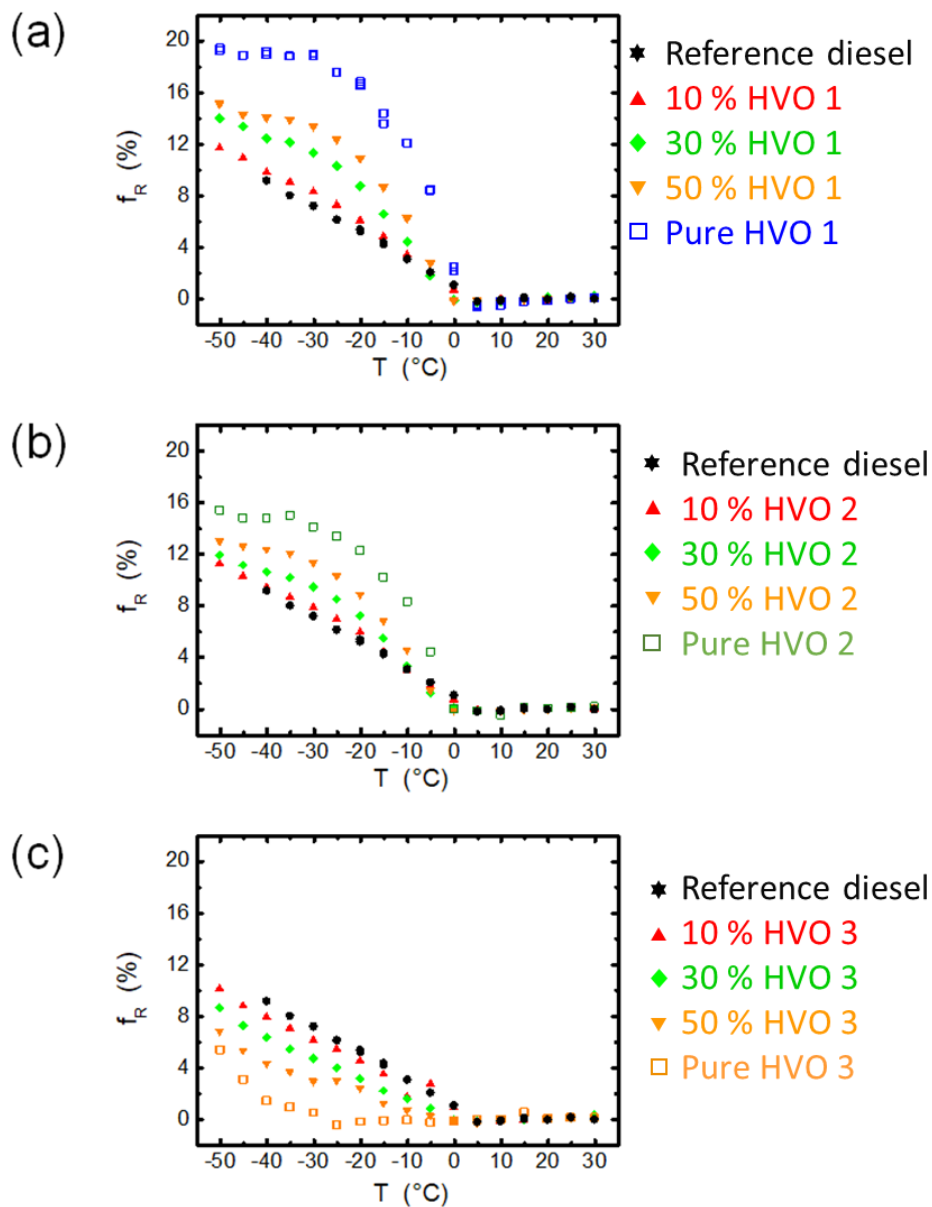
Figure 5. Fraction of protons involved in crystallites formed within blends of the reference diesel and (a) HVO 1, (b) HVO 2 and (c) HVO 3, crystallized at a fixed temperature. The HVO content was set to 10 wt %, 30 wt % and 50 wt %. The data determined on both pure reference diesel and pure HVO were included in the plot, for the sake of comparison. Before the sample crystallization, a heating step at 60°C was applied. Some measurements for the pure HVO 1 curve were repeated for robustness assessment.

For all HVO, the 10% mixed sample displayed a similar f_R pattern as the diesel reference showing that, at this concentration, the HVO have no impact on the diesel cold-flow properties. In Table 2, the cloud point, CFPP, and pour point for the 10% mixed samples determined according to the standards have been reported. These values are indeed comparable to those measured for the diesel.

Table 2. Summary of the cold-flow properties obtained for neat diesel and the 10% mixed samples and the major features derived from SSNMR.

	Cloud point ASTM D7689	Pour point ASTM D7346	CFPP EN116	Solid-state NMR data
				Temperature of apparition of a rigid fraction
Diesel	-3°C	-12°C	-2°C	5°C
10% HVO 1	- 3 °C	- 12 °C	- 3 °C	5°C
10% HVO 2	- 3 °C	- 12 °C	- 3 °C	5°C
10% HVO 3	- 3 °C	- 12 °C	- 3 °C	5°C

In the 30% and 50% mixed samples, the HVO has a clear impact on the $f_R(T)$ pattern as compared to the reference diesel. In contrast to HVO 1 and HVO 2, the temperature below which HVO 3 crystallizes differs from the one determined for the diesel. Interestingly, for the blends based on HVO 3, the onset of crystallization occurs at the same temperature as the one measured for the neat diesel, which suggests that crystallites involving only diesel components are first formed. The temperature at which a rigid fraction is detected is not affected by the blend composition and corresponds to the highest temperature measured for the neat blend components, i.e., that of the diesel (5°C). This observation suggests that blending has no impact on the nucleation step of the crystallization process [17]. However, crystal growth is strongly affected for the mixtures with 30% and 50% of HVO. For these latter, the $f_R(T)$ profile is

intermediate between those of HVO and diesel in the blend. Depending on the nature of the added HVO, a positive or a negative impact on the cold-flow properties is observed.

4. DISCUSSION

Aside from the NMR experiments, the cold-flow properties of the three HVO were also characterized by typical experiments used to document the dynamic behavior of fuels in cold conditions. The cloud point (CP) is the temperature of a diesel fuel at which the smallest observable cluster of wax crystals occurs upon cooling under prescribed conditions. The CP occurs when the temperature of the diesel fuel is low enough to cause wax crystals to precipitate. The pour point (PP) represents the temperature at which a wax crystal structure forms or viscosity increases, or both, and becomes sufficient to impede movement of the surface of the fuel under the conditions of the test. The cold filter plugging point (CFPP) was incorporated because of the failure of CP and PP to completely predict the performance of diesels during cold weather operations [18]. The CFPP corresponds to the lowest temperature at which a given volume of diesel fuel still passes through a standardized filtration device in a specified time when cooled under certain conditions.

The results of these tests for each HVO are summarized in Table 3 and compared to the major characteristics obtained by SSNMR.

Table 3. Summary of the cold-flow properties obtained for pure HVO samples 1 to 3 and the major features derived from SSNMR.

HVO	Cloud point ASTM D7689	Pour point ASTM D7346	Cold filter plugging point EN116	Solid-state NMR data	
				Appearance temperature of a rigid fraction	f_R at -50°C
HVO 1	- 6 °C	- 6 °C	- 8 °C	2 °C	20 %
HVO 2	- 8 °C	- 9 °C	- 9 °C	2 °C	16 %
HVO 3	- 38 °C	- 57 °C	- 39 °C	- 23 °C	6 %

The results of the cold-flow properties of the HVO are in good agreement with the behavior captured by SSNMR experiments, with a significant difference between the low-temperature performances of HVO 3 compared to HVO 1 and 2. The temperature below which a rigid fraction is detected by NMR is however significantly higher than the cloud point, pour point and CFPP. This feature arises from the fact that the MSE experiment allows the detection of weak fractions (as low as a few percent) of protons involved in the crystallites formed during the early stage of crystallization. In other words, the earlier onset of crystallization detected by SSNMR demonstrates the higher sensitivity of this technique to detect rigid fractions compared to more conventional approaches. From another point of view, the value of f_R at low temperature (-50°C) is a way to quantify the propension of a given diesel, HVO or diesel/HVO blend, to crystallize. It is worth mentioning that the difference in the percentage of the rigid fraction at -50°C between HVO 1 and HVO 2 is not accessible to the typical physical tests and is a differentiation-criterion specific to the described SSNMR technique. Beyond these two characteristic values, the whole $f_R(T)$ profile allows to picture the whole crystallization process and particularly to investigate the influence of a given HVO on diesel/HVO blends properties.

In order to establish a relationship between low-temperature properties of the HVO and their chemical composition, both ^1H liquid-state NMR and two-dimensional comprehensive gas

chromatography (GC×GC) experiments of each pure HVO sample were recorded (see Supporting Information). The hydrocarbon chain length, the presence of unsaturated chains, and the level of isomerization were indeed reported to significantly impact the cold-flow properties of HVO [21–24].

^{1}H liquid-state NMR experiments showed that HVO 2 is the only sample containing some residual unsaturated chains with a signal at about 5.5 ppm. The presence of unsaturated chains, mostly when in *cis* conformation, is known to be favorable to low-temperatures properties [19,21]. The presence of unsaturated chains in HVO 2 could account for its lower rigid fraction compared to HVO 1 (16 % compared to 20 % at -50°C).

GC×GC-FID analysis evidenced the presence of n-paraffins and iso-paraffins in the investigated samples and provided the mass distribution of both hydrocarbon families according to the carbon number. The measured total content of n-paraffins vs. iso-paraffins is summarized in Table 4. Besides, well-centered carbon distributions around C16-C18 were obtained (see Supporting Information).

Table 4. Mass repartition between n-paraffins and iso-paraffins observed by GC×GC for each HVO.

HVO	n-paraffins (m/m %)	iso-paraffins (m/m %)
1	34.6	65.3
2	29.7	70.0
3	12.8	87.2

The three investigated HVO samples appear to be mostly composed of iso-paraffins, with iso-paraffins going from 65.3 % (HVO 1) to 70.0 % (HVO 2) and 87.2 % (HVO 3). This composition is the result of the isomerization step occurring during the HVO preparation process.

Isomerization has been suggested as a relevant strategy to improve the cold properties of biodiesels [21,23]. This strategy was found to be especially efficient in the case of long (>C16) chains with a low amount of unsaturations, with cloud point reductions of up to 20°C. The remarkable properties of HVO 3, as visualized by physical tests and by its significantly lower rigid fraction evidenced by SSNMR, is expected to result from its higher branching level. The long chains and the low levels of unsaturations of HVO 3 make isomerization the primary factor impacting the cold-flow properties in this study.

5. CONCLUSION

The ability of an HVO, because of its high branching level, to positively modify the cold-flow properties of petroleum diesels, at blending percentage equal to 30 % and above, was well captured by SSNMR. Isomerization seems to pave the way for reducing the environmental impact of diesels while simultaneously improving their cold-flow properties, provided that the appropriate process and formulation are designed. A deep understanding of the chemical structure and low-temperature physical behaviors, as offered by already-available analytical techniques, is a precious help for the optimization of the next generation of diesels.

Magic-Sandwich Echo SSNMR experiments demonstrated to be highly robust and sensitive in the determination of the crystallized fractions within oil samples such as diesels and hydrotreated vegetable oils. Their ease of implementation and their possible adjustment to benchtop low-field spectrometers make them a promising solution for a broad range of systems and applications.

Supporting Information

Two-dimensional Gas-Chromatography with FID detection: experimental details and results of analysis for HVO 1, HVO 2, HVO 3 and the reference diesel. Optical microscopy: experimental

details and results of analysis for HVO 1, HVO 2, HVO 3 and the reference diesel. [1]H solid-state

NMR experiments: reproducibility investigation, influence of isothermal versus non-isothermal

crystallization on the ^{1}H solid-state NMR experiments. ^{1}H liquid-state NMR: experimental

details and spectra of HVO 1, HVO 2 and HVO 3. Comparison between the cloud point

measurement (ASTM D7689) for diesel/HVO blends and the characterization of their

crystallization behavior by ^{1}H SSNMR.

Acknowledgments

References

(1) *European Commission. Statistical Pocketbook 2019: EU transport in figures. 2019.* https://doi.org/10.2832/017172.

(2) Tinprabath, P.; Hespel, C.; Chanchaona, S.; Foucher, F. Influence of biodiesel and diesel fuel blends on the injection rate under cold conditions. *Fuel* **2015**, *144*, 80–89. DOI: 10.1016/j.fuel.2014.12.010.

(3) Bernardo Tormos; Ricardo Novella; Antonio GarcIa; Kevin Gargar. Comprehensive study of biodiesel fuel for HSDI engines in conventional and low temperature combustion conditions.

(4) Leng, L.; Li, W.; Li, H.; Jiang, S.; Zhou, W. Cold Flow Properties of Biodiesel and the Improvement Methods: A Review. *Energy Fuels* **2020**, *34* (9), 10364–10383. DOI: 10.1021/acs.energyfuels.0c01912.

(5) Lin, H.; Xie, M.; Yin, S.; Yang, T.; Su, B.; Chen, F.; Han, S.; Xue, Y. Influence of Methacrylate-benzyl Methacrylate-N-vinyl-2-pyrrolidone as Pour Point Depression on Cold Flow Properties of Diesel Fuel. *Energy Fuels* **2020**, *34* (2), 1514–1523. DOI: 10.1021/acs.energyfuels.9b03603.

(6) Jiang, Z.; Hutchinson, J. M.; Imrie, C. T. Measurement of the wax appearance temperatures of crude oils by temperature modulated differential scanning calorimetry. *Fuel* **2001**, *80*, 367–371.

(7) Claudy, P.; Létoffé, J.-M.; Neff, B.; Damin, B. Diesel fuels: determination of onset crystallization temperature, pour point and filter plugging point by differential scanning calorimetry. Correlation with standard test methods. *Fuel* **1986**, *65* (6), 861–864. DOI: 10.1016/0016-2361(86)90082-7.

(8) Paso, K.; Kallevik, H.; Sjöblom, J. Measurement of Wax Appearance Temperature Using Near-Infrared (NIR) Scattering. *Energy Fuels* **2009**, *23* (10), 4988–4994. DOI: 10.1021/ef900173b.

(9) Santos, S. M.; Wolf-Maciel, M. R.; Fregolente, L. V. Cold flow properties: Applying exploratory analyses and assessing predictive methods for biodiesel and diesel-biodiesel blends. *Sustainable Energy Technologies and Assessments* **2023**, *57*, 103220. DOI: 10.1016/j.seta.2023.103220.

(10) Hradecká, I.; Velvarská, R.; Jaklová, K. D.; Vráblík, A. Rapid determination of diesel fuel properties by near-infrared spectroscopy. *Infrared Physics & Technology* **2021**, *119*, 103933. DOI: 10.1016/j.infrared.2021.103933.

(11) Wang, S.; Liu, S.; Yuan, Y.; Zhang, J.; Wang, J.; Kong, D. Simultaneous detection of different properties of diesel fuel by near infrared spectroscopy and chemometrics. *Infrared Physics & Technology* **2020**, *104*, 103111. DOI: 10.1016/j.infrared.2019.103111.

(12) Besghini, D.; Mauri, M.; Hashemi, P.; Knarr, M.; Adden, R.; Mischnick, P.; Simonutti, R. Time-Domain NMR Elucidates Fibril Formation in Methylcellulose Hydrogels. *Macromolecules* **2023**, *56* (12), 4694–4704. DOI: 10.1021/acs.macromol.2c02550.

(13) Malmierca, M. A.; González-Jiménez, A.; Mora-Barrantes, I.; Posadas, P.; Rodríguez, A.; Ibarra, L.; Nogales, A.; Saalwächter, K.; Valentín, J. L. Characterization of Network Structure and Chain Dynamics of Elastomeric Ionomers by Means of 1 H Low-Field NMR. *Macromolecules* **2014**, *47* (16), 5655–5667. DOI: 10.1021/ma501208g.

(14) Zhang, R.; Yu, S.; Chen, S.; Wu, Q.; Chen, T.; Sun, P.; Li, B.; Ding, D. Reversible cross-linking, microdomain structure, and heterogeneous dynamics in thermally reversible cross-linked polyurethane as revealed by solid-state NMR. *The journal of physical chemistry. B* **2014**, *118* (4), 1126–1137. DOI: 10.1021/jp409893f. Published Online: Jan. 17, 2014.

(15) Bärenwald, R.; Champouret, Y.; Saalwächter, K.; Schäler, K. Determination of chain flip rates in poly(ethylene) crystallites by solid-state low-field 1H NMR for two different sample morphologies. *The journal of physical chemistry. B* **2012**, *116* (43), 13089–13097. DOI: 10.1021/jp3061625. Published Online: Oct. 22, 2012.

(16) Schäler, K.; Achilles, A.; Bärenwald, R.; Hackel, C.; Saalwächter, K. Dynamics in Crystallites of Poly(ε-caprolactone) As Investigated by Solid-State NMR. *Macromolecules* **2013**, *46* (19), 7818–7825. DOI: 10.1021/ma401532v.

(17) Dwivedi, G.; Sharma, M. P. Impact of cold flow properties of biodiesel on engine performance. *Renewable and Sustainable Energy Reviews* **2014**, *31*, 650–656. DOI: 10.1016/j.rser.2013.12.035.

(18) Dwivedi, G.; Verma, P.; Sharma, M. P. Impact of Oil and Biodiesel on Engine operation in Cold Climatic condition. *J. Mater. Environ. Sci.* **2016**, *7*.

(19) Folayan, A. J.; Anawe, P. A. L.; Aladejare, A. E.; Ayeni, A. O. Experimental investigation of the effect of fatty acids configuration, chain length, branching and degree of unsaturation on biodiesel fuel properties obtained from lauric oils, high-oleic and high-linoleic vegetable oil biomass. *Energy Reports* **2019**, *5*, 793–806. DOI: 10.1016/j.egyr.2019.06.013.

(20) Veríssimo, M.; Gomes, M. T. S. Assessment on the use of biodiesel in cold weather: Pour point determination using a piezoelectric quartz crystal. *Fuel* **2011**, *90* (6), 2315–2320. DOI: 10.1016/j.fuel.2011.02.034.

(21) Hoekman, S. K.; Broch, A.; Robbins, C.; Ceniceros, E.; Natarajan, M. Review of biodiesel composition, properties, and specifications. *Renewable and Sustainable Energy Reviews* **2012**, *16* (1), 143–169. DOI: 10.1016/j.rser.2011.07.143.

(22) Echim, C.; Maes, J.; Greyt, W. de. Improvement of cold filter plugging point of biodiesel from alternative feedstocks. *Fuel* **2012**, *93*, 642–648. DOI: 10.1016/j.fuel.2011.11.036.

 (23) Reaume, S.; Ellis, N. Use of Isomerization and Hydroisomerization Reactions to Improve the Cold Flow Properties of Vegetable Oil Based Biodiesel. *Energies* **2013**, *6* (2), 619–633. DOI: 10.3390/en6020619.